

MOLECULAR HYDROGEN AND ITS IONS IN DARK INTERSTELLAR  
CLOUDS AND STAR FORMING REGIONS

by

Craig Alan Kulesa

---

A Dissertation Submitted to the Faculty of the  
DEPARTMENT OF ASTRONOMY  
In Partial Fulfillment of the Requirements  
For the Degree of  
DOCTOR OF PHILOSOPHY  
In the Graduate College  
THE UNIVERSITY OF ARIZONA

2002



#### STATEMENT BY AUTHOR

This dissertation has been submitted in partial fulfillment of requirements for an advanced degree at The University of Arizona and is deposited in the University Library to be made available to borrowers under rules of the Library.

Brief quotations from this dissertation are allowable without special permission, provided that accurate acknowledgment of source is made. Requests for permission for extended quotation from or reproduction of this manuscript in whole or in part may be granted by the head of the major department or the Dean of the Graduate College when in his or her judgment the proposed use of the material is in the interests of scholarship. In all other instances, however, permission must be obtained from the author.

SIGNED: \_\_\_\_\_

## ACKNOWLEDGMENTS

I'd like to thank my advisor, J. J. Charfman, for...

## DEDICATION

Nuclear war would really set back cable TV. –Ted Turner

## TABLE OF CONTENTS

LIST OF FIGURES . . . . .	9
LIST OF TABLES . . . . .	21
ABSTRACT . . . . .	23
1 INTRODUCTION . . . . .	24
1.1 Importance of H <sub>2</sub> and its ions H <sub>2</sub> <sup>+</sup> and H <sub>3</sub> <sup>+</sup> . . . . .	25
1.2 Spectroscopy of H <sub>2</sub> and its Ions: Observational Challenges . . . . .	27
1.2.1 H <sub>2</sub> Spectroscopy . . . . .	29
1.2.2 Spectroscopy of H <sub>2</sub> <sup>+</sup> and H <sub>3</sub> <sup>+</sup> . . . . .	34
1.3 Observations of H <sub>2</sub> and H <sub>3</sub> <sup>+</sup> . . . . .	36
1.4 Dissertation Overview and Direction . . . . .	42
2 DIRECT MEASUREMENT OF MOLECULAR HYDROGEN AND ITS IONS IN INTERSTELLAR CLOUDS AND STAR-FORMING REGIONS . . . . .	46
2.1 Indirect Measurements of H <sub>2</sub> & H <sub>3</sub> <sup>+</sup> . . . . .	48
2.1.1 CO as a tracer of H <sub>2</sub> . . . . .	48
2.1.2 Extinction Mapping of Molecular Clouds . . . . .	49
2.1.3 Submillimeter continuum emission from dust as a probe of H <sub>2</sub> . . . . .	50
2.2 Outline: Direct Observations of H <sub>2</sub> and H <sub>3</sub> <sup>+</sup> . . . . .	51
2.3 Presentation of Observational Data . . . . .	55
2.3.1 Source Selection . . . . .	55
2.3.2 Observations . . . . .	60
2.3.3 Data Reduction . . . . .	61
2.3.4 Presentation of Spectra . . . . .	64
2.4 Analysis and Results . . . . .	69
2.4.1 Curve of Growth Analysis for the CO Lines . . . . .	86
2.4.2 Analysis of H <sub>2</sub> Detections in Dense Clouds . . . . .	100
2.4.3 Analysis of H <sub>3</sub> <sup>+</sup> Detections in Dense Clouds . . . . .	105
2.5 Discussion . . . . .	106
2.5.1 The Abundances of <sup>12</sup> CO, <sup>13</sup> CO, H <sub>2</sub> and H <sub>3</sub> <sup>+</sup> . . . . .	106
2.6 Conclusions . . . . .	120
3 PHOTODISSOCIATION MODELS AND PHYSICAL STRUCTURE OF THE $\rho$ OPHI- UCHI MOLECULAR CLOUD . . . . .	122
3.1 Submillimeter Spectral Line Mapping of the $\rho$ Oph Cloud . . . . .	126
3.1.1 Presentation of Observations . . . . .	126
3.2 The Gaseous Environment of Elias 29 . . . . .	138

TABLE OF CONTENTS — CONTINUED		
3.2.1	Line Excitation and Radiative Transfer . . . . .	138
3.2.2	Comparison of Infrared and Submillimeter Observations . .	141
3.2.3	Disentangling Multiple Cloud Components toward Elias 29	142
3.3	Morphology of the $\rho$ Oph Cloud . . . . .	148
3.3.1	Large Scale CO and [C I] Emission . . . . .	148
3.3.2	Structure of the $\rho$ Oph A Cloud Core . . . . .	152
3.4	PDR Modeling of the $\rho$ Oph Cloud . . . . .	159
3.4.1	Vicinity of the $\rho$ Oph A Core . . . . .	159
3.4.2	Other ISO positions . . . . .	169
3.4.3	Directly Probing the Western H <sub>2</sub> PDR Front . . . . .	171
3.5	Summary . . . . .	175
4	FORMATION, EXCITATION AND SURVIVAL OF MOLECULAR HYDROGEN AND ITS IONS IN HOSTILE ENVIRONMENTS . . . . .	180
4.1	The Origin of H <sub>3</sub> <sup>+</sup> in Circumstellar Disks . . . . .	182
4.1.1	Are the Observed Lines Due to H <sub>3</sub> <sup>+</sup> ? . . . . .	183
4.1.2	Thermalized H <sub>3</sub> <sup>+</sup> line emission . . . . .	188
4.1.3	Non-Thermal H <sub>3</sub> <sup>+</sup> Excitation . . . . .	195
4.2	H <sub>2</sub> in the Crab Nebula . . . . .	197
4.2.1	Infrared H <sub>2</sub> imaging of the Crab . . . . .	197
4.2.2	Spectroscopic Observations of H <sub>2</sub> toward Filament FK-10 . .	200
4.2.3	H <sub>2</sub> Excitation Analysis . . . . .	203
4.2.4	H <sub>2</sub> Formation Mechanisms in the Crab . . . . .	211
4.3	Is H <sub>2</sub> <sup>+</sup> Observable? . . . . .	213
4.4	Summary . . . . .	213
5	SHOCKED AND FLUORESCENT MOLECULAR HYDROGEN LINE EMISSION FROM THE ARP 299 MERGER SYSTEM . . . . .	217
5.1	Introduction . . . . .	217
5.2	Presentation of Observational Data . . . . .	220
5.2.1	Observations . . . . .	220
5.2.2	Data Reductions . . . . .	221
5.2.3	Presentation of Spectra . . . . .	226
5.3	The Nature of the H <sub>2</sub> Excitation . . . . .	242
5.3.1	Extinction . . . . .	242
5.3.2	UV intensity . . . . .	248
5.3.3	Determination of Excitation Mechanism . . . . .	248
5.3.4	H <sub>2</sub> Luminosity . . . . .	257
5.4	Analysis of the Fluorescent and Shocked H <sub>2</sub> in Arp 299 . . . . .	258
5.4.1	Modeling Fluorescent H <sub>2</sub> Emission . . . . .	258

## TABLE OF CONTENTS — CONTINUED

5.4.2	Limitations and Tests of the H <sub>2</sub> Fluorescence Model . . . . .	270
5.4.3	Shocked H <sub>2</sub> Emission in Arp 299 . . . . .	273
5.5	Concluding Remarks and Acknowledgments . . . . .	280
<b>A</b>	<b>A GUIDE TO REDUCING DATA TAKEN WITH THE PHOENIX INFRARED SPECTROMETER . . . . .</b>	<b>282</b>
A.1	Introduction . . . . .	282
A.2	Outline of the Basic Steps for Phoenix Data Reduction . . . . .	283
A.3	About the Spectra used in this Tutorial . . . . .	284
A.4	Making IRAF go . . . . .	285
A.5	Combining Dark Frames . . . . .	288
A.6	Constructing a Flat Field Frame . . . . .	289
A.6.1	Combining Images: . . . . .	289
A.6.2	Subtracting Dark Current: . . . . .	291
A.6.3	Normalizing the Flat to Unity: . . . . .	291
A.6.4	Removing the Broad Spectral Response: . . . . .	291
A.7	Selecting Images for Bulk Processing . . . . .	293
A.7.1	Method 1: Using Observing Logs . . . . .	294
A.7.2	Method 2: Using Image Headers . . . . .	295
A.8	Sky Subtraction, Flat Fielding and Trimming . . . . .	295
A.9	Aligning Images for Combining . . . . .	298
A.10	Combining Images . . . . .	299
A.11	Extracting a 1D spectrum . . . . .	302
A.12	Removal of Atmospheric Features . . . . .	309
A.13	Wavenumber Calibration . . . . .	315
<b>B</b>	<b>A GUIDE TO REDUCING SPECTROSCOPIC DATA TAKEN AT THE HHT . . . . .</b>	<b>318</b>
B.1	Outline . . . . .	318
B.2	Introduction . . . . .	319
B.2.1	Things to ponder... . . . . .	319
B.3	Installing GILDAS software . . . . .	321
B.4	Basic Reduction of Data from a Single Pointing . . . . .	323
B.4.1	Step 1: Loading CLASS and accessing your data file . . . . .	323
B.4.2	Step 2: Extracting Relevant Spectra . . . . .	325
B.5	Processing of Regularly-Sampled Spectral Line Maps . . . . .	334
B.6	Reduction of Randomly-Sampled On-The-Fly Maps . . . . .	338
B.7	Making Journal-Ready Plots . . . . .	343
B.8	Exporting Data in FITS Format for other Programs . . . . .	345

## LIST OF FIGURES

<p>1.1 Weighing the elemental universe. Big Bang nucleosynthesis formed hydrogen, helium, and a small amount of lithium. <math>10^{10}</math> yr of stellar evolution and enrichment of the interstellar gas has added carbon, nitrogen, oxygen, magnesium, silicon and iron to the scales, in addition to trace amounts of numerous other species – but hydrogen still outweighs them all. . . . .</p> <p>1.2 Simplified chemical networks for carbon (overlap with oxygen in red), nitrogen (overlap with carbon in red) and oxygen (overlap with carbon in red), adapted from Prasad, Tarafdar, Villere, &amp; Huntress (1987). The role of <math>H_2</math> and <math>H_3^+</math> as the initiators of the gas phase chemistry in each network is highlighted in blue bold strokes. . . .</p> <p>1.3 Potential energy curves for the ground state and first two bound excited states of the hydrogen molecule. Spectroscopic notation for the electronic states are labeled, as are the vibrational levels for <math>J = 0</math>. Vibrational level representations for the overlapping excited states are shortened for readability. . . . .</p> <p>1.4 Partial energy level diagram for common rotational and rovibrational lines of <math>H_2</math>. . . . .</p> <p>1.5 Principal vibrational modes of <math>H_3^+</math>. a: “Breathing” <math>v_1</math> mode; infrared inactive. b &amp; c: Infrared active, degenerate <math>v_{2x}</math> and <math>v_{2y}</math> vibrational modes. These occur in combination and are therefore collectively referred to as the <math>v_2</math> mode. . . . .</p> <p>1.6 Energy level diagram of the <math>v_2</math> vibrational mode transitions of <math>H_3^+</math> as observed near <math>4 \mu m</math>. These five transitions represent all observed lines discussed in this dissertation. . . . .</p>	<p style="margin-top: 0;">25</p> <p style="margin-top: 0;">28</p> <p style="margin-top: 0;">29</p> <p style="margin-top: 0;">32</p> <p style="margin-top: 0;">36</p> <p style="margin-top: 0;">37</p>
---	---

## LIST OF FIGURES — CONTINUED

1.7 Sample FUSE spectra of the Lyman (2,0) through (5,0) bands at high and low S/N, from Rachford et al. (2002). <i>Top:</i> HD 210839 with a peak S/N of $24 \text{ pixel}^{-1}$ , $A_V = 1.57 \text{ mag.}$ , $\log N(\text{H}_2) = 20.84$ . <i>Bottom:</i> HD 210839 with a peak S/N $\approx 2 \text{ pixel}^{-1}$ , $A_V = 2.48 \text{ mag.}$ , $\log N(\text{H}_2) = 21.16$ . Note that the $J = 0, 1$ levels are heavily damped and blended, and careful curve fitting is necessary to extract column densities. . . . .	39
2.1 Synthetic $\text{H}_2$ spectra of the $v = 1 - 0$ $S(0)$ line at $2.223 \mu\text{m}$ for $\text{H}_2$ column densities of $1 \times 10^{22}$ , $5 \times 10^{22}$ , and $1 \times 10^{23} \text{ cm}^{-3}$ with $T = 20 \text{ K}$ and an intrinsic linewidth of $1.6 \text{ km s}^{-1}$ , corresponding to a Doppler parameter $b = 1 \text{ km s}^{-1}$ . Spectra include a specified amount of Gaussian noise, and are convolved to spectroscopic resolving powers $R = \lambda/\Delta\lambda$ of 5,000 and 50,000. The weakness of $\text{H}_2$ spectral features, and the necessity of high resolving power is emphasized. . . . .	53
2.2 Spectra of $^{12}\text{CO}$ in the (2,0) R-band; R(0) through R(5). The uppermost spectrum is a typical comparison spectrum of the B2V star $\beta_1 \text{ Sco}$ that depicts the atmospheric transmission. The spectra are the ratioed (corrected) spectra of obscured (young) stellar objects that demonstrate prominent $^{12}\text{CO}$ absorption. The observed velocity shifts are due to the orbital motion of the Earth along the line of sight. . . . .	65
2.3 Spectrum of GL 490 in the $^{12}\text{CO}(2,0)$ R-branch. This represents the combination of two integrations with different grating angles. . . . .	66
2.4 Spectrum of GL 2591 in the $^{12}\text{CO}(2,0)$ R-branch. This represents the combination of two integrations with different grating angles. . . . .	67
2.5 Spectrum of NGC 2024 IRS 2 in the $^{12}\text{CO}(2,0)$ high-J R-branch. This spectrum extends Figure 2.2 and the spectrum depicted in Black & Willner (1984). . . . .	68

## LIST OF FIGURES — CONTINUED

- 2.6 Portion of the spectrum of NGC 2264 IRS 1 in the vicinity of the  $^{13}\text{CO}$  (1,0) R(3) and R(4) lines at  $4.73\ \mu\text{m}$ ; the comparison spectrum is of  $\alpha\ \text{CMa}$ . The effectiveness of the telluric correction is evident here; atmospheric features are canceled to better than 1 part in 200, with the S/N of the spectrum merely going to zero in saturated telluric lines. . . . . 69
- 2.7 Spectrum of  $\zeta\ \text{Oph}$  in the  $^{12}\text{CO}$  (1,0) R-branch. Symbols depict “features” of low S/N due to telluric absorption lines. The R(0) and R(1) lines of  $^{12}\text{CO}$  are clearly observed. . . . . 70
- 2.8 Detections of  $\text{H}_2$  (1,0) S(0) absorption in dark molecular clouds: the top plot represents the atmospheric transmission, ratioed astronomical spectra follow. The spectra obtained toward NGC 2024 IRS 2 at two different epochs can be compared to the landmark observations performed by Lacy, Knacke, Geballe, & Tokunaga (1994). In this plot and those to follow, asterisks show the  $V_{\text{LSR}}$  of CO absorption in each source. . . . . 71
- 2.9 Sample observations of  $\text{H}_2$  (1,0) S(1) in dark molecular clouds: the top plot represents the atmospheric transmission, ratioed astronomical spectra follow. NGC 2024 IRS 2 and GL 2591 show  $\text{H}_2$  absorption at the  $V_{\text{LSR}}$  of the  $^{12}\text{CO}$  absorption; other sources show  $\text{H}_2$  emission from hot gas along the line of sight. . . . . 72
- 2.10 Observations of the ortho-para doublet of  $\text{H}_3^+$  at  $2725.9\ \text{cm}^{-1}$  and  $2726.2\ \text{cm}^{-1}$  in dark molecular clouds: the top plot represents the atmospheric transmission, ratioed astronomical spectra follow. NGC 2264 IRS 1 does not show any  $\text{H}_3^+$  absorption. . . . . 73
- 2.11 Observations of the  $R(1,1)^l$  para line of  $\text{H}_3^+$  at  $2691.45\ \text{cm}^{-1}$  in dark molecular clouds: the top plot represents the atmospheric transmission, ratioed astronomical spectra follow. No detections are claimed for MonR2 IRS 3 and NGC 2264 IRS 1. . . . . 74

## LIST OF FIGURES — CONTINUED

2.12 Curve of growth analysis for CO along the line of sight toward NGC 2024 IRS 2, for $b = 0.55 \text{ km s}^{-1}$ . . . . .	89
2.13 Curve of growth analysis for CO along the line of sight toward NGC 2024 ID197, for $b = 1.5 \text{ km s}^{-1}$ . . . . .	89
2.14 Linear curve of growth analysis for CO along the line of sight toward AFGL 490, for $b = 0.55 \text{ km s}^{-1}$ . The fit's poor quality suggests multiple excitation components along the line of sight, demonstrated in the right figure by a simple-minded but incorrect two-component fit. . . . .	90
2.15 Complete two component curve of growth analysis for AFGL 490. Note that the cold gas is 20K colder, and the warm gas 10K warmer than by blindly fitting two independent temperature components to the derived column densities (Figure 2.14). . . . .	91
2.16 Linear curve of growth analysis for the ambient cloud CO at a $V_{\text{LSR}} = -7 \text{ km s}^{-1}$ along the line of sight toward AFGL 2591, for $b = 4.5 \text{ km s}^{-1}$ . The poor fit quality suggests multiple excitation components along the line of sight, demonstrated in the right-hand figure by a simple-minded but incorrect two-component fit. . . . .	92
2.17 Complete two component curve of growth analysis for AFGL 2591. Note that the cold gas is 10K colder, and the warm gas 30K warmer than by blindly fitting two independent temperature components to the derived column densities (Figure 2.16). . . . .	93
2.18 Single component curve of growth analysis of the high velocity ( $V_{\text{LSR}} = -25 \text{ km s}^{-1}$ gas associated with the protostellar outflow of AFGL 2591. The derived CO temperature agrees with the $^{13}\text{CO}$ $v = (1,0)$ data of Mitchell et al. (1989). . . . .	94
2.19 Curve of growth analysis for CO along the line of sight toward NGC 2264 IRS 1, for $b = 3.0 \text{ km s}^{-1}$ . . . . .	95

## LIST OF FIGURES — CONTINUED

2.20	Curve of growth analysis for CO along the line of sight toward S140 IRS 1, for $b = 3.0 \text{ km s}^{-1}$ . . . . .	96
2.21	Curve of growth analysis for CO along the line of sight toward Elias 29, for $b = 1.6 \text{ km s}^{-1}$ . . . . .	96
2.22	Curve of growth analysis for CO along the line of sight toward SVS 20, for $b = 1.0 \text{ km s}^{-1}$ . . . . .	103
2.23	Curve of growth analysis for $^{12}\text{CO}$ (1,0) along the line of sight toward the diffuse cloud $\zeta$ Oph, for $b = 0.8 \text{ km s}^{-1}$ . A $3\sigma$ upper limit on the detection of the R(2) line is plotted. We do not expect to have observed this line. . . . .	104
2.24	Plot of $[^{12}\text{CO}/^{13}\text{CO}]$ abundance as a function of CO excitation temperature for several lines of sight. Error bars reflect $1\sigma$ uncertainties mostly in the comparison of $^{13}\text{CO}$ observations made one decade ago with a facility FTS at the CFHT by Mitchell et al. (1989, 1990); Mitchell & Maillard (1993); Mitchell et al. (1995). . . . .	109
2.25	Photometrically-derived estimates of $A_v$ for each source are plotted against the column of hydrogen nuclei estimated from the cold absorbing H <sub>2</sub> detected in this study. The straight line is the standard dust-to-extinction conversion of Bohlin, Savage & Drake (1978), simply plotted (unfit) across the data. . . . .	114
2.26	Integrated line intensity ratios for the $J = 1 \rightarrow 0$ , $3 \rightarrow 2$ and $4 \rightarrow 3$ transitions of H $^{13}\text{CO}^+$ , as applied to NGC 2024 IRS 2 (T=50K), in the optically-thin limit. . . . .	119

## LIST OF FIGURES — CONTINUED

3.1	Contextual overview of the main $\rho$ Oph cloud. The grayscale image 870 $\mu\text{m}$ continuum map from Johnstone et al. (2000), atop which the locations of infrared sources, cloud cores, and the extent of our spectral line submillimeter maps are annotated. A region of infrared H <sub>2</sub> emission indicative of a PDR front is labeled by a quadrilateral.	132
3.2	40' $\times$ 40' map centered near infrared source WL1 in CO(4 $\rightarrow$ 3) (a) and [C I]( $^3P_1 \rightarrow ^3P_0$ ) (b). For CO(4 $\rightarrow$ 3) contours are in steps of $9\sigma=7$ K km s $^{-1}$ starting at 20 K km s $^{-1}$ . For [C I]( $^3P_1 \rightarrow ^3P_0$ ) contours are in steps of $4\sigma=2$ K km s $^{-1}$ starting at 6 K km s $^{-1}$ .	133
3.3	5' $\times$ 5' map from the HHT toward Elias 29 in CO(3 $\rightarrow$ 2). Contours are in steps of 10 K km s $^{-1}$ starting at 30 K km s $^{-1}$ . Spectra at 5 representative positions are depicted, with axis values ranging from $-5 < V_{LSR} < 15$ (km s $^{-1}$ ) and $-2 < T_a^* < 21$ (K).	134
3.4	5' $\times$ 5' and 6' $\times$ 5' maps from the HHT toward WL16 in C <sup>18</sup> O (2 $\rightarrow$ 1) and HCO $^+$ (3 $\rightarrow$ 2). Sample spectra at the offset of Elias 29 (90'', 10'') are depicted above; the velocity scale is $-1 < V_{LSR} < 9$ (km s $^{-1}$ ) and the $T_a^*$ scale is 2K, 2K, and 0.5K per major division for C <sup>18</sup> O(2 $\rightarrow$ 1), HCO $^+$ (3 $\rightarrow$ 2) and HCO $^+$ (4 $\rightarrow$ 3), respectively.	135
3.5	$\sim$ 5' $\times$ 5' maps toward position EW4. in CO(2 $\rightarrow$ 1) (left) and <sup>13</sup> CO(2 $\rightarrow$ 1) (right). For CO(2 $\rightarrow$ 1), contours are in steps of $15\sigma=5.5$ K km s $^{-1}$ starting at 5.5 K km s $^{-1}$ . For <sup>13</sup> CO(2 $\rightarrow$ 1), contours are in steps of $9\sigma=3.9$ K km s $^{-1}$ starting at 6.5 K km s $^{-1}$ . For C <sup>18</sup> O(2 $\rightarrow$ 1) contours are in steps of $6\sigma=1.6$ K km s $^{-1}$ starting at 4 K km s $^{-1}$ . For CS(5 $\rightarrow$ 4) contours are in steps of $1.5\sigma=2$ K km s $^{-1}$ starting at 4 K km s $^{-1}$ . Contours for HCO $^+$ (3 $\rightarrow$ 2) and HCO $^+$ (4 $\rightarrow$ 3) are in steps of 2.5 K km s $^{-1}$ starting at 4 K km s $^{-1}$ .	136

## LIST OF FIGURES — CONTINUED

- 3.6  $5' \times 5'$  and  $8' \times 5'$  maps from the HHT toward ISO EW5 in (a)  $\text{C}^{18}\text{O}(2 \rightarrow 1)$  and (b)  $\text{HCO}^+(3 \rightarrow 2)$ . (c)  $3' \times 6'$  map from the HHT toward the  $\rho$  Oph A cloud core, offset from ISO EW5, in  $\text{HCO}^+(4 \rightarrow 3)$ . Contours are spaced 5, 4, and 3 K km s $^{-1}$ , starting at 5, 5, and 6 K km s $^{-1}$ , respectively. . . . . 137
- 3.7 Comparison of escape probability level populations with LTE as a function of energy above the ground state, adopting  $n = 10^4$  cm $^{-3}$  and  $T_k = 25\text{K}$ , for column densities scaled from  $N(\text{H}_2) = 2.5 \times 10^{22}$  cm $^{-2}$ . LTE is a good approximation for the level populations of  $\text{C}^0$ ,  $\text{C}^+$ , and low-J CO in dark clouds. LTE is not palatable for species with high excitation conditions, which may be subthermally excited. . . . . 140
- 3.8 Physical conditions derived for the line of sight to Elias 29 from the integrated intensities of  $\text{HCO}^+ 3 \rightarrow 2$  and  $4 \rightarrow 3$  in the escape-probability formalism. The three tracks represent different abundances of  $\text{HCO}^+$ , and the length of the tracks represents the span of parameter space that reproduce the  $\text{HCO}^+$  line ratios. An abundance of  $\leq 3 \times 10^{-9}$  allows subthermal excitation of  $\text{HCO}^+$  that matches CO, whose excitation temperature is plotted as a horizontal line, flanked by  $1\sigma$  dotted lines. Higher abundances, limited by the nondetection of  $\text{H}^{13}\text{CO}^+$ , indicate colder conditions than demonstrated by CO. . . . . 146
- 3.9 Overlay of the AST/RO [C I] ( ${}^3P_1 \rightarrow {}^3P_0$ ) map contours atop the Abergel et al. (1996) ISOCAM image at 7 & 15  $\mu\text{m}$ . The [C I] emission is extended and generally follows the edges of warm dust emission expected for the illuminated surface of the molecular cloud. Crosses indicate cloud cores identified in Figure 3.1. The thick oval highlights a region of intense  $\text{H}_2$  and PAH emission indicative of a  $\text{H}_2$  photodissociation front, from Boulanger et al. (1999). . . . . 149

## LIST OF FIGURES — CONTINUED

- 3.10 AST/RO spectra of optically-thick CO( $4 \rightarrow 3$ ) across the  $\rho$  Oph molecular cloud, resampled to a  $4'$  grid for readability. Although the line profiles are severely self-absorbed over the majority of the main cloud, Gaussian line profiles are observed throughout the periphery and yield estimates of the kinetic temperature. As in Figures 3.2 and 3.9, offsets are relative to the map center near infrared source WL1. The velocity width for each spectrum is  $9 \text{ km s}^{-1}$ , and the corrected main beam temperature scale goes from -3 to 30K. . . . . 150
- 3.11 HHT spectra of optically-thick CO and  $^{13}\text{CO}$  in the ( $2 \rightarrow 1$ ) transition toward the ISO EW4 position; integrated intensity maps may be found in Figure 3.5. Line profiles have been resampled to a  $50''$  grid for readability. As in Figure 3.5, offsets are relative to the EW4 map center of Liseau et al. (1999). For the CO map, the velocity width for is  $25 \text{ km s}^{-1}$ , and the corrected main beam temperature scale goes from -4 to 40K. For  $^{13}\text{CO}$ , the velocity width is  $15 \text{ km s}^{-1}$  per spectrum, and the corrected brightness temperature scale goes from -4 to 30K. . . . . 154
- 3.12 The bottom panels show a plot of optical depth through the  $^{13}\text{CO}$  ( $2 \rightarrow 1$ ) and  $\text{HCO}^+$ ( $3 \rightarrow 2$ ) lines, assuming  $\frac{N(^{13}\text{CO})}{N(\text{C}^{18}\text{O})} = 7.1$  and  $\frac{N(\text{HCO}^+)}{N(\text{H}^{13}\text{CO}^+)} = 70$ . The spectra used to create these profiles are displayed in the top panels. . . . . 155
- 3.13 Physical conditions derived from the integrated intensities of  $\text{HCO}^+$   $3 \rightarrow 2$  and  $4 \rightarrow 3$  in the escape-probability formalism, for the southwest corner of the  $\text{HCO}^+$  “ring” (EW4 offset  $0'', 60''$ ). Four tracks represent different abundances of  $\text{HCO}^+$ , and the length of the tracks represents the span of parameter space that fit the available observations. An abundance of  $3 \times 10^{-9}$  best matches the column density of  $\text{H}^{13}\text{CO}^+$  if the isotopomer ratio is 70. The excitation temperature of CO is plotted as a horizontal line, flanked by  $1\sigma$  uncertainties as dotted lines. . . . . 157

## LIST OF FIGURES — CONTINUED

3.14 HHT spectra of $\text{HCO}^+$ ( $4 \rightarrow 3$ ) toward the $\rho$ Oph A cloud core, offset coordinates are from the ISO EW5 position of Liseau et al. (1999). Integrated intensity maps may be found in Figure 3.4. Line profiles have been resampled to a $40''$ grid for readability. The velocity width is $10 \text{ km s}^{-1}$ per spectrum, and the corrected brightness temperature scale ranges from -4 to 15K. . . . .	159
3.15 Composite spectra from the HHT (with convolved $\theta_{FWHM} = 3.5'$ ) plotted on same velocity axis as the AST/RO CO( $4 \rightarrow 3$ ) and [C I] lines. . . . .	160
3.16 Depth dependence of hydrogen abundances for the best fit PDR model: $n_{\text{H}} = 2 \times 10^4 \text{ cm}^{-3}$ and $I_{\text{UV}} = 30$ for the ISO-EW4 pointing within the $\rho$ Oph cloud. . . . .	165
3.17 Illustration of a clumpy PDR and the physical region each emission line probes. . . . .	169
3.18 Intensities of $158\mu\text{m}$ [C II], $63\mu\text{m}$ [O I] and $609\mu\text{m}$ [C I] line emission along the ISO east-west cross-section of the $\rho$ Oph cloud . . . .	171
3.19 Synthetic spectrum of $\text{H}_2$ emission at $2 \mu\text{m}$ , observed with a resolving power of 2000. Solid line: ultraviolet pumped radiative excitation; Dotted line: thermal emission at $T=2000\text{K}$ . The intensity scale for both plots is scaled to the brightness of the 1-0 S(1) line. . . . .	173
3.20 Schematic diagram of the $\rho$ Oph dark cloud, with PDR surfaces highlighted in black. The concave back side of the cloud, per Liseau et al. (1999), bears the bulk of the UV radiation field from HD 147889. However, if the extinction toward the $\text{H}_2$ emission (Boulanger et al. 1999) is low, the “filament” PDR on the western edge of the dense molecular cloud likely represents a foreground PDR region that is not shadowed from HD 147889 by the rest of the cloud. The depicted dark cloud is also surrounded by a diffuse “halo” of gas and dust. . . . .	176

## LIST OF FIGURES — CONTINUED

4.1	CSHELL/IRTF spectra of emission lines coincident with the Q(1,0) and Q(3,0) lines of $\text{H}_3^+$ in the circumstellar disk around the Herbig AeBe star HD 141569. Atmospheric features are modeled and superimposed as a solid red line. . . . .	184
4.2	NIRSPEC/Keck spectra of CO emission lines in the Herbig AeBe stars AB Aur and HD 141569. Excitation of the CO in AB Aur is due to resonant scattering, however in HD 141569 it is due to the pumping of CO electronic energy levels by ultraviolet photons from HD 141569 itself. Atmospheric features are modeled and superimposed as a solid red line. . . . .	185
4.3	Synthetic LTE spectra of $\text{H}_3^+$ , for $\text{N}(\text{H}_3^+) = 10^{12} \text{ cm}^{-2}$ and warm gas $< 500 \text{ K}$ . . . . .	192
4.4	Synthetic LTE spectra of $\text{H}_3^+$ , for $\text{N}(\text{H}_3^+) = 10^{12} \text{ cm}^{-2}$ and hot gas $> 500 \text{ K}$ . . . . .	193
4.5	Narrow-band, continuum-subtracted image of the Crab Nebula in the $2.122 \mu\text{m}$ (1,0) S(1) line of $\text{H}_2$ . . . . .	198
4.6	Overlay of the $\text{H}_2$ image from Figure 4.5 in the vicinity of the FK-6 filament, atop the $1.644 \mu\text{m}$ [Fe II] image contours from Graham, Wright, & Longmore (1990). The box dimensions are $75'' \times 75''$ , tick-marks are $5''$ each. North is up, east is left. . . . .	199
4.7	K-band spectrum of the FK-10 filament peak, with $\text{H}_2 v = 1 \rightarrow 0$ , $2 \rightarrow 1$ and $3 \rightarrow 2$ transitions marked . . . . .	201
4.8	Two-dimensional spectral images of He I $2.058 \mu\text{m}$ and $\text{H}_2$ (1,0) S(1) line emission. Note the dispersion in linewidths and the position dependence of the velocity shifted gas along the N/S-positioned slit, and the $> 1000 \text{ km s}^{-1}$ magnitude of the shifts, both redward (toward the top of the image) and blueward (toward the bottom). . .	202

## LIST OF FIGURES — CONTINUED

4.9	Calculation of H <sub>2</sub> dissociation rate as function of cloud depth, including dust opacity and H <sub>2</sub> self-shielding. The dotted line represents the depth at which the typical H <sub>2</sub> lifetime equals the age of the Crab Nebula – the dashed line represents an H <sub>2</sub> lifetime against UV dissociation that is ten times the age of the Crab. . . . .	209
4.10	Calculation of H <sub>2</sub> <sup>+</sup> frequencies, transition probabilities and thermalized emissivities for $T = 500$ K. . . . .	215
5.1	apertures1.eps . . . . .	223
5.2	apertures2.eps . . . . .	224
5.3	K-band spectrum of Arp 299 A (IC 694). In this spectrum and those to follow, a low-order fit to the stellar continuum has been subtracted.	227
5.4	K-band spectrum of Arp 299 A, aperture centered 6.6'' NE (see Figure 5.1). . . . .	228
5.5	K-band spectrum of Arp 299 B2, centered 2.5'' NW of the nucleus (see Figure 5.2). . . . .	229
5.6	K-band spectrum of Arp 299 B1 and B2. . . . .	230
5.7	K-band spectrum of Arp 299 C and C'. . . . .	231
5.8	H-band spectrum of Arp 299 A, B1 and B2 . . . . .	232
5.9	H-band spectrum of Arp 299 C and C' . . . . .	233
5.10	Geometry of the UV-fluorescence starburst model. Above is the standard model with stars and gas scattered randomly throughout the aperture. Below are two alternative models: in model B the stars and gas are more intimately associated such that the mean UV radiation field intercepting molecular clouds, $I_{UV}$ , is doubled, in model C they are anti-correlated such that $I_{UV}$ is halved. . . . .	268
A.1	Acquisition image of S140 IRS 1 with Phoenix . . . . .	285
A.2	Launching IRAF from the Redhat Programs menu . . . . .	286
A.3	Fitting the spectral response of a flat field frame . . . . .	293
A.4	A sample flat field, before running <code>response</code> . . . . .	294
A.5	A raw 600-second exposure of S140 IRS 1 from the 2-meter . . . . .	296

## LIST OF FIGURES — CONTINUED

A.6	The same frame after sky subtraction of adjacent frames . . . . .	298
A.7	Using <code>splot</code> on the squashed image for alignment . . . . .	300
A.8	The composition of eight, 600-second exposures . . . . .	303
A.9	Defining an aperture for extracting a 1D spectrum . . . . .	307
A.10	The interactive tracing of the continuum across the array . . . . .	308
A.11	The extracted spectrum, looking mostly like the atmosphere... . . .	309
A.12	A naive telluric correction; not very good... . . . . .	310
A.13	Running the <code>telluric</code> task . . . . .	313
A.14	The spectrum after telluric correction, nice! . . . . .	315
A.15	As sent to ApJ! How far we've come... . . . . .	317
B.1	A CO study of the NGC 2024 cloud core, taken at the HHT in 1997 and 1998. . . . .	320
B.2	A digital sky survey image of the Arp 299 system of merging galax- ies (also known as NGC 3690 or Markarian 171). The data we will analyze comes from the pointing labeled by the black circle. . . . .	324
B.3	A quick look at two subscans of HHT data. . . . .	328
B.4	An example of a bad scan averaged into the accumulated data. . . . .	330
B.5	Summed, unsmoothed data with bad scan dropped. . . . .	331
B.6	The final, smoothed spectrum of Arp 299 A in the CO $J = 3 \rightarrow 2$ line. . . . .	332
B.7	Spectral line map of $\rho$ Oph in the 492 GHz fine structure $J = 1 \rightarrow 0$ line of atomic carbon. . . . .	336
B.8	Publishable color image of [C I] toward $\rho$ Oph. . . . .	339
B.9	On-the-fly $\text{HCO}^+$ $J = 4 \rightarrow 3$ map of $\rho$ Oph . . . . .	343
B.10	Publishable, annotated on-the-fly map of $\text{HCO}^+$ in $\rho$ Oph. . . . .	345
B.11	Example of a PGPLT figure made by exporting CLASS data as ASCII text or in FITS format. . . . .	346

## LIST OF TABLES

1.1	Thermalized H <sub>2</sub> line emission . . . . .	33
2.1	Log of Infrared Observations by Object . . . . .	57
2.1	Log of Infrared Observations by Object . . . . .	58
2.1	Log of Infrared Observations by Object . . . . .	59
2.2	Comparison Stars for Telluric Absorption Correction . . . . .	62
2.3	Observed Absorption Lines Toward NGC 2024 IRS 2 . . . . .	76
2.4	Observed Absorption Lines Toward NGC 2024 ID 197 . . . . .	77
2.5	Observed Absorption Lines Toward NGC 2264 IRS 1 . . . . .	78
2.6	Observed Absorption Lines Toward AFGL 2591 . . . . .	79
2.7	Observed Absorption Lines Toward AFGL 490 . . . . .	80
2.8	Observed Absorption Lines Toward S140 IRS 1 . . . . .	81
2.9	Observed Absorption Lines Toward SVS 20 . . . . .	81
2.10	Observed Absorption Lines Toward Elias 29 . . . . .	82
2.11	Absorption Lines Observed Toward Other Sources . . . . .	83
2.11	Absorption Lines Observed Toward Other Sources . . . . .	84
2.12	Transition Frequencies and Oscillator Strengths for CO, H <sub>2</sub> & H <sub>3</sub> <sup>+</sup> . . . . .	85
2.12	Transition Frequencies and Oscillator Strengths for CO, H <sub>2</sub> & H <sub>3</sub> <sup>+</sup> . . . . .	86
2.13	<sup>12</sup> CO, <sup>13</sup> CO Column Densities and Temperatures . . . . .	98
2.14	Measured H <sub>2</sub> Column Densities . . . . .	103
2.15	Measured H <sub>3</sub> <sup>+</sup> Column Densities . . . . .	107
2.16	Abundances of <sup>12</sup> CO, <sup>13</sup> CO, H <sub>2</sub> and H <sub>3</sub> <sup>+</sup> . . . . .	110
2.17	Adopted maximal abundances for destroying H <sub>3</sub> <sup>+</sup> . . . . .	117
2.18	Measurements of $\zeta_0$ in Dense Clouds . . . . .	119
3.1	Summary table of submillimeter observations. . . . .	128
3.1	Summary table of submillimeter observations. . . . .	129
3.2	Derived Column Densities of Cold Gas Toward Elias 29 . . . . .	143
3.3	Resulting column densities toward ISO-EW4. . . . .	161
3.4	Homogeneous PDR model results for ISO-EW4 . . . . .	163
3.5	Inhomogeneous PDR, contrast = 30: $3 \times 10^3 \text{ cm}^{-3}$ & $10^5 \text{ cm}^{-3}$ . . . . .	166
3.6	Inhomogeneous PDR, contrast = 1000: $10^3 \text{ cm}^{-3}$ & $10^6 \text{ cm}^{-3}$ . . . . .	166
3.7	PDR Modeling of a $\rho$ Oph cross-section; $n = 10^4 \text{ cm}^{-3}$ . . . . .	170
3.8	H <sub>2</sub> $v = 1 \rightarrow 0$ line ratios as a function of increasing extinction . . . . .	174
4.1	Observed Interstellar Molecular Ions . . . . .	181
4.2	Atomic lines adjacent to the purported H <sub>3</sub> <sup>+</sup> lines . . . . .	187
4.3	Atomic lines adjacent to the unidentified line at $2507.5 \text{ cm}^{-1}$ . . . . .	187
4.4	Selected [Ti II] lines from the $15265.62 \text{ cm}^{-1}$ upper state . . . . .	188

## LIST OF TABLES — CONTINUED

4.5	Using H <sub>3</sub> <sup>+</sup> as a rotational thermometer . . . . .	191
4.6	H <sub>2</sub> Excitation Models for Filament FK-10 . . . . .	205
4.7	Shielded H <sub>2</sub> dissociation rates as a function of cloud depth . . . . .	208
4.8	Simulated spectrum of H <sub>2</sub> <sup>+</sup> . . . . .	214
5.1	Log of Infrared Observations . . . . .	222
5.2	Observed Spectral Lines in Arp 299 A . . . . .	235
5.2	Observed Spectral Lines in Arp 299 A . . . . .	236
5.3	Observed Spectral Lines in Arp 299 B1 . . . . .	237
5.4	Observed Spectral Lines in Arp 299 B2 . . . . .	238
5.5	Observed Spectral Lines in Arp 299 C . . . . .	239
5.6	Observed Spectral Lines in Arp 299 C' . . . . .	240
5.7	Observed Spectral Lines in Arp 299 non-nuclear apertures . . . . .	241
5.7	Observed Spectral Lines in Arp 299 non-nuclear apertures . . . . .	242
5.8	Extinction Estimates for Arp 299 . . . . .	246
5.8	Extinction Estimates for Arp 299 . . . . .	247
5.9	Extinction Models for Arp 299 A . . . . .	249
5.10	H <sub>2</sub> Excitation Models for Arp 299 A . . . . .	253
5.11	H <sub>2</sub> Excitation Models for Arp 299 B1 . . . . .	254
5.12	H <sub>2</sub> Excitation Models for Arp 299 C . . . . .	255
5.13	H <sub>2</sub> Excitation Models for Arp 299 C' . . . . .	256
5.14	Properties of Early-Type Stars . . . . .	259
5.15	UV-Fluorescence Model Results for Arp 299 . . . . .	264
5.15	UV-Fluorescence Model Results for Arp 299 . . . . .	265
5.16	H <sub>2</sub> shock model results . . . . .	278
5.17	Summary of model results for Arp 299 <sup>a</sup> . . . . .	279

## ABSTRACT

Fundamental observations of molecular hydrogen ( $H_2$ ) in dark clouds, star forming regions, and radiation-dominated environments are presented, modeled, and interpreted. Through a weak infrared absorption line spectrum, the abundance of cold  $H_2$  in dark molecular clouds and star forming regions is measured directly and compared with the abundance of its most commonly cited surrogate, CO. The derived abundance of CO is between 1.5 and  $2.5 \times 10^{-4}$  for the sample. The CO molecule thus represents about  $\frac{1}{3}$  of the total carbon budget in dense clouds. Also detected via infrared line absorption is the pivotal molecular ion  $H_3^+$ , yielding a direct measure of the cosmic ray ionization rate of  $H_2$  in dark molecular clouds (between 1 and  $5 \times 10^{-17} s^{-1}$ ), a process that instigates the complex ion-neutral chemical pathways that form many of the 120+ known molecular species deep inside interstellar clouds. These timely tests of theory are applied to the detailed submillimeter-wave study of the  $\rho$  Ophiuchi star forming cloud and photodissociation front, allowing partial disentanglement of the complicated physical and chemical structure of a star forming cloud. Yet  $H_2$  and  $H_3^+$  continue to surprise and delight us with more mysteries. The formation, excitation and survival of molecules in unusual & hostile environments is highlighted by the discoveries of  $H_3^+$  in circumstellar disks of early-type stars, and of fluorescing  $H_2$  in two harshly-irradiated filaments of the Crab Nebula. The role of  $H_3^+$  as a possible tracer of planet formation, and the evolution of  $H_2$  in the interstellar medium is discussed. The study of  $H_2$  in hostile environments is extended to the ensemble properties of extragalactic star forming regions, and applied to the Arp 299 merger system as a unique probe of the feedback of newly-formed hot stars, their fossil remains, and the molecular material which formed them.

## CHAPTER 1

### INTRODUCTION

*I write about molecules with great diffidence, having not yet rid myself of the tradition that atoms are physics, but molecules are chemistry, but the new conclusion that hydrogen is abundant seems to make it likely that the above-mentioned elements H, O, and N will frequently form molecules.*

Sir Arthur Eddington (1937)

Recognition of the existence of interstellar molecules and their importance to all aspects of astrophysics has reached a critical mass. The humble beginnings of astrochemistry, marked by the detection of interstellar CN, CH and  $\text{CH}^+$  absorption lines at visible wavelengths toward background stars in the late 1930's, have given way to a renaissance of discovery and the formation of an interdisciplinary field, astrochemistry, whose grasp reaches from comets to cosmology, from meter-wave radio wavelengths to X-rays, from simple diatomic molecules to organic species approaching the complexity of amino acids, in environments ranging from cold and quiescent to violently hostile and dynamic. It is now well accepted that molecular interactions, both with radiation and each other, provide a unique observational and theoretical tool of unprecedented diagnostic power. It is less often realized that the mere existence of molecules, through their pivotal effects on their environment's ionization and thermal balance, can strongly regulate their dynamical and chemical evolution. Indeed, exploration and definition of this facet of molecular astrophysics may well be its ultimate contribution to the whole of astrophysics.

### 1.1 Importance of H<sub>2</sub> and its ions H<sub>2</sub><sup>+</sup> and H<sub>3</sub><sup>+</sup>

Theoretical and observational evidence has established that 90 percent (by number) of the known baryonic matter in the Universe is composed of elemental hydrogen (Boesgaard & Steigman, 1985; Peebles, 1993). The astronomer's periodic table is therefore an unusual sight to traditional physicists and chemists (Figure 1.1). Therefore, of the 123 interstellar molecules reported to date (Wootten, A., 2002), it is fully expected that the hydrogen molecule (H<sub>2</sub>) is by far the dominant constituent of astrophysical plasmas. Indeed, the contribution of H<sub>2</sub> to the total baryonic mass of the Universe is predicted to be secondary only to atomic hydrogen, helium, and their ions. Furthermore, molecular hydrogen has the unique and pivotal distinction of being the gaseous state of hydrogen that gives rise to the formation of stars.

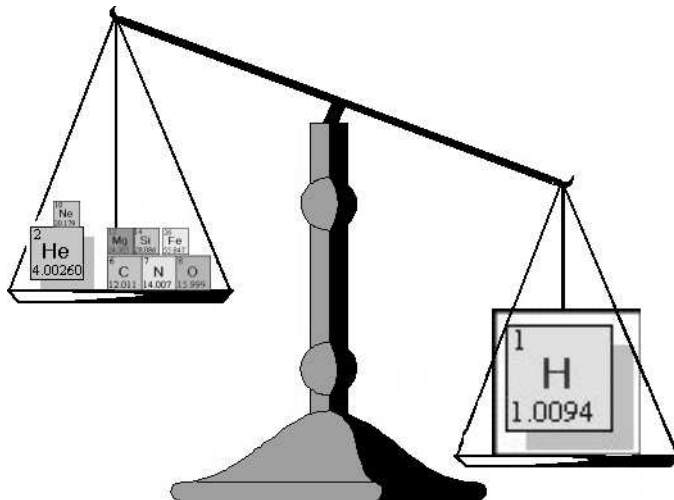


Figure 1.1: Weighing the elemental universe. Big Bang nucleosynthesis formed hydrogen, helium, and a small amount of lithium. 10<sup>10</sup> yr of stellar evolution and enrichment of the interstellar gas has added carbon, nitrogen, oxygen, magnesium, silicon and iron to the scales, in addition to trace amounts of numerous other species – but hydrogen still outweighs them all.

Interstellar gas is continuously replenished by the final phases of stellar evolution, principally the mass loss of asymptotic giant branch (AGB) stars and envelope ejection of supernovae explosions (Spitzer, 1978). The conversion of interstellar gas from atomic to molecular form depends primarily upon sufficient gas and dust density and the strength of the ambient interstellar radiation field. The phase transition from atomic to molecular gas in interstellar clouds is sharply defined, generally dictated by radiative processes, and hence described as a photon-dominated region, or photodissociation region (PDR) (Tielens & Hollenbach, 1985; Black & van Dishoeck, 1987; Draine & Bertoldi, 1996). Not only does H<sub>2</sub> dominate the mass of such molecular clouds, but the thermal balance of its formation energy and emission of radiation at infrared wavelengths plays a significant role in the physical state and evolution of such clouds. Indeed, the formation of all stars from dense condensations in molecular clouds gives H<sub>2</sub> special importance in the complicated symbiosis of the interstellar medium (ISM) of the Galaxy and the stars that form from it. As primordial species in the gas dominated post-recombination Universe, H<sub>2</sub> provided new mechanisms of heating and cooling which played a role in the formation of the very first star forming structures which led, either eventually or contemporaneously, to the formation of the first galaxies (Anninos & Norman, 1996; Norman & Spaans, 1997; Haiman, Abel, & Rees, 2000; Hutchings, Santoro, Thomas, & Couchman, 2002). The critical role of H<sub>2</sub> as star-forming fuel therefore has significant cosmological implications.

The role of the ions derived from H<sub>2</sub> are no less important. The ionization of H<sub>2</sub> by photons of energy 15.4 eV or greater, most typically by the local production of X-rays and energetic cosmic rays, results in the creation of H<sub>2</sub><sup>+</sup>. H<sub>2</sub><sup>+</sup> is very short lived in the interstellar medium, reacting with nearly every collision partner it encounters. In dense molecular clouds, the most probable reaction is with H<sub>2</sub>, re-

sulting in the production of  $\text{H}_3^+$  (Martin, McDaniel, & Meeks, 1961), which in turn represents the cornerstone of the gas phase reaction networks that initiate the formation of most other molecules in interstellar space (Figure 1.2). In the absence of ultraviolet (UV) radiation in the dark interiors of molecular clouds, the  $\text{H}_2$  ionization rate therefore defines the energetic chemical processes that form most other molecules (Herbst & Klemperer, 1973). Therefore, the measurement of  $\text{H}_3^+$  in concert with  $\text{H}_2$  represents the most direct confirmation of the gas phase production of molecules by measurement of the cosmic ray ionization rate of  $\text{H}_2$  that initiates these chemical networks. Similarly,  $\text{H}_2^+$ ,  $\text{H}_3^+$  and their daughter ions partially control the ionization fraction in molecular clouds, which in turn regulates the ability of a molecular cloud condensation to withstand self-gravitational collapse to form new stars and planets due to interaction with magnetic fields. Owing to their relative simplicity among molecules,  $\text{H}_2$ ,  $\text{H}_2^+$  and  $\text{H}_3^+$  also represent our best theoretical models of the quantum mechanical structure of molecules, and the subsequent spectroscopic tests of such theories in both Earth-based and interstellar laboratories have an important, ongoing history.

Okay, that's enough. I quit. :)

But first, here's a random table!

Table 1.1. Thermalized H<sub>2</sub> line emission

T(K)	$I_{S(0)}$	$I_{1-0\ S(1)}$	$I_{tot}$
10	5.9248e-25	0.0	5.9248e-25
20	6.9748e-14	0.0	6.9748e-14
50	2.3665e-07	0.0	2.3774e-07
100	1.8863e-05	0.0	3.2499e-05
150	6.7871e-05	9.9590e-18	3.4086e-04
200	1.2315e-04	8.1477e-13	1.3739e-03
300	2.1476e-04	6.0481e-08	7.5244e-03
500	3.2295e-04	3.9785e-04	6.2136e-02
1000 <sup>b</sup>	4.2691e-04	2.1145e-01	2.1839e+00
2000 <sup>b</sup>	4.8601e-04	3.3212e+00	3.9504e+01
3000 <sup>b</sup>	5.0667e-04	6.7842e+00	2.2498e+02

<sup>a</sup>All intensities in erg s<sup>-1</sup> cm<sup>-2</sup> sr<sup>-1</sup> for a N(H<sub>2</sub>)= 10<sup>22</sup> cm<sup>-2</sup> thick plane-parallel slab

<sup>b</sup>High temperatures are likely to only apply to the surfaces of interstellar clouds, not to an entire “dark” cloud

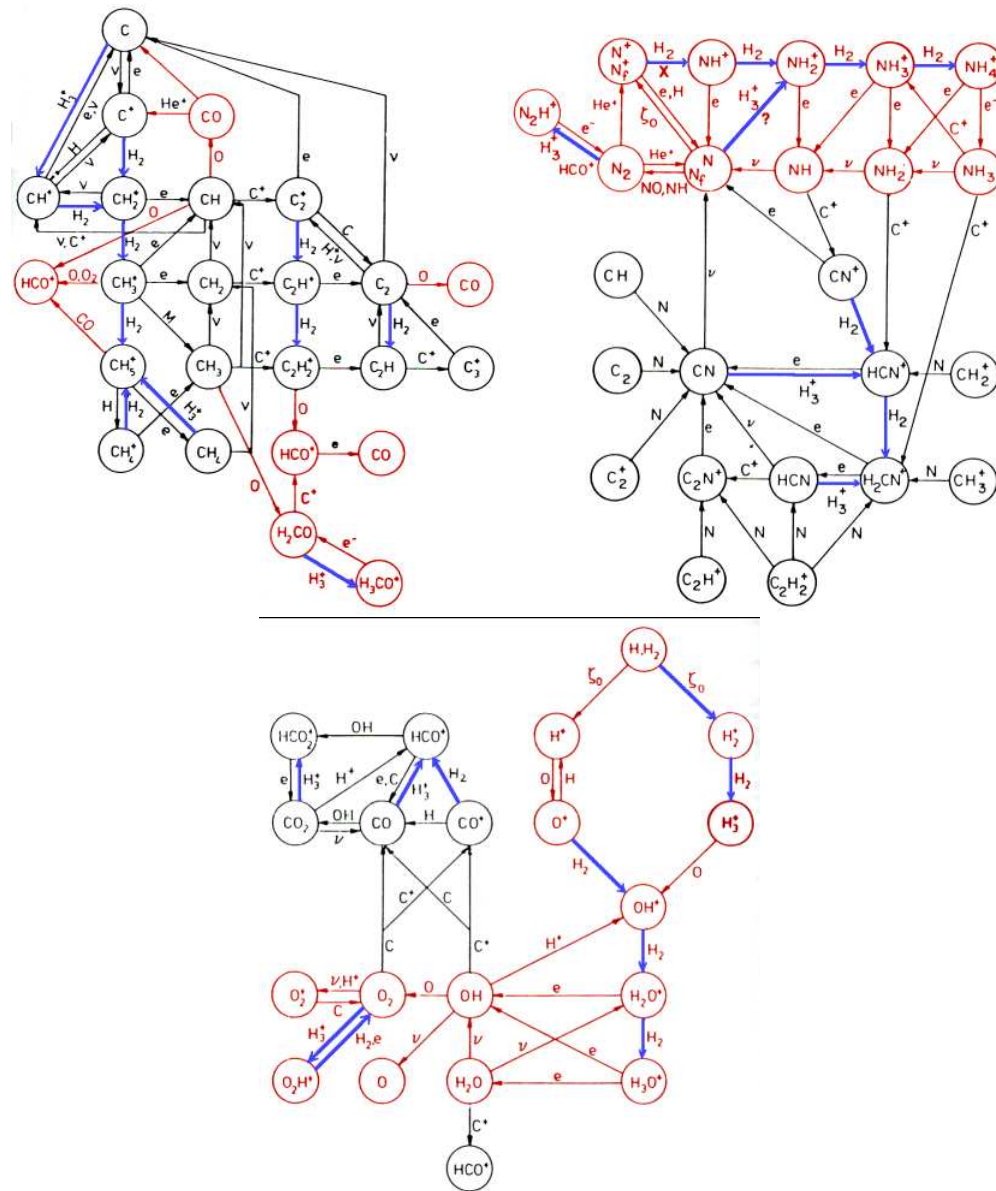


Figure 1.2: Simplified chemical networks for carbon (overlap with oxygen in red), nitrogen (overlap with carbon in red) and oxygen (overlap with carbon in red), adapted from Prasad, Tarafdar, Villere, & Huntress (1987). The role of H<sub>2</sub> and H<sub>3</sub><sup>+</sup> as the initiators of the gas phase chemistry in each network is highlighted in blue bold strokes.

## CHAPTER 2

### DIRECT MEASUREMENT OF MOLECULAR HYDROGEN AND ITS IONS IN INTERSTELLAR CLOUDS AND STAR-FORMING REGIONS

*Unfortunately, because they are mostly composed of molecular hydrogen ( $H_2$ ) and also because they are so cold, 99% of a molecular cloud's mass is virtually undetectable by means of direct observations.*

ESO Press Release 29a-c/99

To date, over 120 different molecules have been detected in the interstellar medium, and some, such as the common molecular ion  $HCO^+$ , have been identified in space before being synthesized on Earth. Through their spectra, these interstellar molecules provide a wide range of diagnostic probes of conditions in molecular clouds and star-forming regions; through their interactions with radiation and with each other, they also partly regulate the dynamical evolution of interstellar clouds.

Although most interstellar molecules have been detected through emission line spectroscopy at millimeter wavelengths, this technique is inapplicable to non-polar molecules like  $H_2$ ,  $CO_2$ ,  $C_2H_2$ , and  $H_3^+$ , which are thought to be central to our understanding of interstellar chemistry. In particular,  $H_2$  comprises the vast majority of the mass in star-forming molecular clouds, a large fraction of the interstellar mass of the Galaxy, and plays a significant role in the heating and cooling, and hence *evolution* of interstellar gas. All stars, as far as we know, are born from dense, dark molecular clouds whose hydrogenic contents

are composed almost entirely of H<sub>2</sub>. The role of protonated H<sub>2</sub>, H<sub>3</sub><sup>+</sup>, is no less significant. H<sub>3</sub><sup>+</sup> is the cornerstone of interstellar chemistry responsible for initiating the gas-phase chemical networks that form many of the observed molecules in dark clouds (Herbst & Klemperer, 1973; Watson, 1976). H<sub>3</sub><sup>+</sup> forms from H<sub>2</sub> by the cosmic ray ionization of H<sub>2</sub> to H<sub>2</sub><sup>+</sup>:



The first reaction is slow; a typical H<sub>2</sub> molecule in the ISM will be ionized once every billion years. Once H<sub>2</sub><sup>+</sup> forms however, only 10<sup>5</sup> seconds elapses before it reacts with the first available species, typically another H<sub>2</sub> molecule. Thus, the ionization of H<sub>2</sub> results in the efficient and rapid production of H<sub>3</sub><sup>+</sup>. Measurement of H<sub>3</sub><sup>+</sup> provides the most direct measurement of this fundamental process that initiates chemical models of interstellar clouds and star forming regions.

The physical symmetry of H<sub>2</sub> and H<sub>3</sub><sup>+</sup> give them vanishingly small permanent dipole moments and therefore do not allow for a traditional rotational emission line spectrum at radio wavelengths. Hopes for detecting the dominant H<sub>2</sub> molecule in cold clouds are frustrated further by its low moment of inertia, which yields large rotational energy level spacings that are energetically unreachable to cold hydrogen molecules in molecular clouds (see Introduction). Direct measurements of H<sub>2</sub> in its ortho- and para- ground states are made possible by a dipole-permitted electronic absorption line spectrum in the vacuum ultraviolet between 912 and 1130 Å. Although such observations, made possible by space-borne telescopes like *Copernicus* and FUSE, are critical to assessing the chemistry and contents of diffuse clouds, they are inapplicable to studies of the dense, dark

clouds where stars are formed. Thus, indirect measures of the abundance of H<sub>2</sub> have been necessary.

Okay, that's enough of that. Get the idea? :)

## APPENDIX A

# A GUIDE TO REDUCING DATA TAKEN WITH THE PHOENIX INFRARED SPECTROMETER

This document is available online in browsable (color) format at:

<http://loke.as.arizona.edu/~ckulesa/phoenix/reduction/>

### A.1 Introduction

Phoenix is a cryogenic, long slit, high resolution infrared spectrograph designed for use at the f/15 focus of the KPNO 2.1-meter, the KPNO, CTIO and SOAR 4-meter, and the Gemini 8-meter telescopes. For more instrument details, consult the Phoenix Web Page and the Phoenix Instrument Manual.

This document graphically describes the data reduction process, following the reduction of a complete dataset to a publishable result, and includes a Phoenix IRAF package containing tasks to speed along the data reduction process. It documents a method of data reduction which is robust and highly optimized for getting the most from Phoenix data. It is certainly not the only way, but it should save you a lot of time. If you find a way to improve the techniques provided here, I want to know!

It is designed to complement the NOAO data reduction exercise, which nicely covers general aspects of spectroscopic reduction in IRAF, but not the more spe-

cific issues of IR data reduction as pertains to Phoenix data. For example, successful reduction of pre-2001 Phoenix data (with the old Aladdin I array) critically hinges upon careful bad pixel rejection and image combination, which isn't discussed at all.

This exercise uses a basic installation of IRAF, the Image Reduction and Analysis Facility (some say, It Reeks And Fumes), although new reduction pipelines that operate independently of IRAF (using PDL and Python) are in development. Until such pipelines are completed, basic IRAF functionality is necessary.

## A.2 Outline of the Basic Steps for Phoenix Data Reduction

- Make IRAF go
- Combine Dark Frames [`imcombine`]
- Construct Flat Field Frame:
  - Combine flat field frames [`imcombine`]
  - Subtract dark frame [`imarith`]
  - Normalize image to unity [`imarith`]
  - Correct for spectral response [`response`]
- Selecting Files for Bulk Processing
- Sky-subtract, Flat-field + Trim data frames [`phxproc`]
- Combining frames:
  - Squashing images to measure offsets [`squash`, `splot`]
  - Expanding and aligning images [`strexp`, `nalign`]

- Combining frames, removing spectral tilt & bad pixels [mask, ircombine]
- Contracting images to original scale [contract]
- Extraction of 1D spectra: [apall]
  - Defining apertures [apedit]
  - Tracing spectra [aptrace]
  - Extraction and 2nd pass at removing bad pixels [apextract]
  - Reviewing your spectrum [splot]
- Telluric Correction [telluric]
- Wavelength Calibration [identify, refspec, dispcor]
- Getting Data out of IRAF [wspectext]

### A.3 About the Spectra used in this Tutorial

We will be processing data taken after the clearing of monsoon storms on the morning of 2000 July 16, at the venerable Kitt Peak 2.1-meter telescope. The data is of a heavily-embedded young stellar object S140 IRS 1 in the L1204 molecular cloud (Cepheus). It is a 7th magnitude source at the 2.34 micron ( $4272\text{ cm}^{-1}$ ) wavelength of the R-branch of the first overtone  $^{12}\text{CO}$  band. Owing to the high degree of obscuration, we expect to see the signature of interstellar CO absorption lines along this line of sight. We are using the spectrum of Deneb (which was at a similar elevation at the time of observations) as a comparison spectrum to remove atmospheric features. The data are composed of eight 600-second exposures, with "seat of pants" guiding as this source is optically invisible. Slit losses due to inaccurate guiding are estimated to be 20-30%; pretty good considering! Note

that these data were taken with the "old" *Aladdin I* array, and with multiple-sampling (i.e. 4 Low Noise Reads), about 5% of the array's pixels are bad and must be discarded. This dataset therefore represents an instructive challenge, as improper rejection of bad pixels will yield useless results.

Below is an image of S140 IRS 1 at 2.34 microns, taken with Phoenix in imaging mode during target acquisition.

## REFERENCES

- Aalto, A., Black, J. H., Booth, R. S., and Johansson, L. E. B. 1991, *A&A*, 247, 291
- Aalto, A., Black, J. H., Johansson, L. E. B., and Booth, R. S. 1991, *A&A*, 249, 323
- Aalto, S., Booth, R. S., Black, J. H., Koribalski, B., Wielebinski, R. 1994, *A&A*, 286, 365.
- Aalto, S., Booth, R. S., Black, J. H., Johansson, L. E. B. 1995, *A&A*, 300, 369.
- Aalto, S., Radford, S. J. E., Scoville, N. Z., Sargent, A. I. 1997, *ApJ*, 475, L107.
- Aaronson, M., Black, J. H., & McKee, C. F. 1974, *ApJL*, 191, L53
- Aaronson, M. 1977, PhD Thesis, Harvard Univ., Cambridge, MA.
- Abergel, A. et al. 1996, *A&A*, 315, L329
- Adams, N. G. & Smith, D. 1981, *ApJ*, 248, 373
- Adams, N. G., & Smith, D. 1984, *Chem. Phys. Lett.*, 105, 604
- Aitken, D. K., Roche, P. F., Allen, M. C., Phillips, M. M. 1982, *MNRAS*, 199, 31.
- Allen, D. A. 1972, *ApJL*, 172, L55
- Alves, J. ;, Lada, C. J., & Lada, E. A. 1999, *ApJ*, 515, 265
- André, P., Ward-Thompson, D. & Barsony, M. 1993, *ApJ*, 406, 122
- Anicich, V. G. & Huntress, W. T. 1986, *ApJS*, 62, 553
- Anninos, P. & Norman, M. L. 1996, *ApJ*, 460, 556

- Armus, L., Heckman, T. M., Weaver, K. A., Lehnert, M. D. 1995, *ApJ*, 445, 666.
- Augarde, R., Lequeux, J. 1985, *A&A*, 147, 273.
- Bally, J., Stark, A. A., Wilson, R. W., & Langer, W. D. 1987, *ApJ*, 312, L45
- Barnstedt, J., Gringel, W., Kappelmann, N., & Grewing, M. 2000, *A&AS*, 143, 193
- Bechtold, J. 1999, H<sub>2</sub> in Space, meeting held in Paris, France, September 28th - October 1st, 1999. Eds.: F. Combes, G. Pineau des Forêts. Cambridge University Press, Astrophysics Series,
- Beck, S. C., Turner, J. L., Ho, P. T. P. 1986, *ApJ*, 309, 70.
- Beck, S. C., Turner, J. L., Ho, P. T. P., Lacy, J.H., Kelly, D. M. 1996, *ApJ*, 457, 610.
- Becklin, E. E., Matthews, K., Neugebauer, G., Willner, S. P. 1978, *ApJ*, 220, 831.
- Beckwith, S. V. W., Sargent, A. I., Chini, R. S., & Guesten, R. 1990, *AJ*, 99, 924
- Bergin, E. A., Ungerechts, H., Goldsmith, P. F., Snell, R. L., Irvine, W. M. & Schloerb, F. P. 1997, *ApJ*, 482, 267
- Black, J. H. & Dalgarno, A. 1976, *ApJ*, 203, 132
- Black, J. H. & Dalgarno, A. 1977, *ApJS*, 34, 405
- Black, J. H., van Dishoeck, E. F., Willner, S. P., & Woods, R. C. 1990, *ApJ*, 358, 459
- Black, J. H. & van Dishoeck, E. F. 1987, *ApJ*, 322, 412
- Black, J. H. & Willner, S. P. 1984, *ApJ*, 279, 673
- Black, J.H. & van Dishoeck, E.F. 1988, *ApJ*, 331, 986.

- Black, J. 1999, H<sub>2</sub> in Space, meeting held in Paris, France, September 28th - October 1st, 1999. Eds.: F. Combes, G. Pineau des Forêts. Cambridge University Press, Astrophysics Series,
- Blair, W. P., Long, K. S., & Raymond, J. C. 1996, ApJ, 468, 871
- Blitz, L. & Williams, J. P. 1997, ApJL, 488, L145
- Boesgaard, A. M. & Steigman, G. 1985, ARA&A, 23, 319
- Bohlin, R. C., Savage, B. D., & Drake, J. F. 1978, ApJ, 224, 132
- Boissé, P. 1990, A&A, 228, 483
- Boogert, A. C. A., Tielens, A. G. G. M., Ceccarelli, C., Boonman, A. M. S., van Dishoeck, E. F., Keane, J. V., Whittet, D. C. B., & de Graauw, T. 2000, A&A, 360, 683
- Boulanger, F., Abergel, A., Falgarone, E., Habart, E., Pineau Des Forêts, G., & Verstraete, L. 1999, H<sub>2</sub> in Space, meeting held in Paris, France, September 28th - October 1st, 1999. Eds.: F. Combes, G. Pineau des Forêts. Cambridge University Press, Astrophysics Series, E34
- Brittain, S. D. & Rettig, T. W. 2002, Nature, 418, 57
- Burton, M. G., Geballe, T. R., Brand, P. W. J. L., Webster, A.S. 1988, MNRAS, 231, 617.
- Burton, M. G., Hollenbach, D. J., & Tielens, A. G. G. M. 1990, ApJ, 365, 620
- Calzetti, D., Kinney, A. L., Storchi-Bergmann, T. 1994, ApJ, 429, 582.
- Calzetti, D., Kinney, A. L., Storchi-Bergmann, T. 1996, ApJ, 458, 132.

- Cardelli, J. A. & Wallerstein, G. 1986, *ApJ*, 302, 492
- Cardelli, J. A., Meyer, D. M., Jura, M., & Savage, B. D. 1996, *ApJ*, 467, 334
- Carr, J.S., Evans II, N.J., Lacy, J.H.& Zhou, S., 1995, *ApJ*, 450, 667.
- Carra, P., Hollenbach, D. J., Lord, S. D., Colgan, S. W. J., Haas, M. R. , Rubin, R. H., Erickson, E. F. 1994, *ApJ*, 423, 223.
- Carrasco, L., Strom, S. E., & Strom, K. M. 1973, *ApJ*, 182, 95
- Carruthers, G. R. 1970, *ApJL*, 161, L81
- Ceccarelli, C., Caux, E., White, G. J., Molinari, S., Furniss, I., Liseau, R., Nisini, B., Saraceno, P., Spinoglio, L., & Wolfire, M. 1998, *A&A*, 331, 372
- Chandler, C. J., Carlstrom, J. E., & Scoville, N. Z. 1995, *ApJ*, 446, 793
- Cernicharo, J., Liu, X.-W., Gonzalez-Alfonso, E., Cox, P., Barlow, M. J., Lim, T., & Swinyard, B. M. 1997, *ApJL*, 483, L65
- Chernoff, D. F., McKee, C. F., Hollenbach, D. J. 1982, *ApJ*, 259, L97.
- Chlewicki, G., and Greenberg, J. M. 1984, *MNRAS*, 210, 791.
- Crutcher, R. M. & Chu, Y. 1985, *ApJ*, 290, 251
- Dalgarno, A. & Stephens, T. L. 1970, *ApJL*, 160, L107
- de Jong, T., Boland, W., & Dalgarno, A. 1980, *A&A*, 91, 68
- Dickman, R. L. 1978, *ApJS*, 37, 407
- Dinerstein, H. L., Lester, D. F., Carr, J. S., Harvey, P. M. 1988, *ApJ*, 327, 27.
- Doherty, R. M., Puxley, P. J., Lumsden, S. L., Doyon, R. 1995, *MNRAS*, 277, 577.

Doty, S. D., van Dishoeck, E. F., van der Tak, F. F. S., & Boonman, A. M. S. 2002,  
*A&A*, 389, 446

Doyon, R., Joseph R. D., Wright, G. S. 1994, *ApJ*, 421, 101.

Doyon, R., Wright, G. S., Joseph, R. D. 1991, *ApJ*, 397, 117.

Doyon, R., Wright, G. S., Joseph, R. D. 1994, *ApJ*, 421, 115.

Draine, B. T., Roberge, W. G., Dalgarno, A. 1983, *ApJ*, 264, 485.

Draine, B.T., and Lee, H.M. 1984, *ApJ*, 285, 89.

Draine, B. T. & Bertoldi, F. 1996, *ApJ*, 468, 269

Drossart, P. et al. 1989, *Nature*, 340, 539

Duley, W. W., Hartquist, T. W., Sternberg, A., Wagenblast, R., & Williams, D. A. 1992, *MNRAS*, 255, 463

Eddington, A. S. 1937, *The Observatory*, 60, 99

Elias, J.H. 1980, *ApJ*, 241, 728.

Elitzur, M., & Netzer, H. 1985, *ApJ*, 291, 464.

Engargiola, G., Zmuidzinas, J., & Lo, K. Y. 1994, *Review of Scientific Instruments*, 65, 1833

Engelbracht, C. W., Rieke, M. J., Rieke, G. H., & Latter, W. B. 1996, *ApJ*, 467, 227.

Falgarone, E., Pineau des Forets, G., & Roueff, E. 1995, *A&A*, 300, 870

Farrenq, R., Guelachvili, G., Sauval, A. J., Grevesse, N., & Farmer, C. B. 1991, *J. Molec. Spectrosc.*, 149, 375

- Felisenfeld, F. C. 1976, ApJ, 209, 638
- Ferland, F. J., 1996, Hazy: A Brief Introduction ot CLOUDY, University of Kentucky Department of Physics and Astronomy Internal Report.
- Fesen, R. A. & Kirshner, R. P. 1982, ApJ, 258, 1
- Field, G. B., Somerville, W. B., & Dressler, K. 1966, ARA&A, 4, 207
- Fischer, J., Simon, M., Benson, J., Solomon, P. M. 1983, ApJ, 273, 27.
- Fischer, J., Geballe, T.R., Smith, H.A., Simon, M., and Storey, J.W.V. 1987, ApJ, 320, 667.
- Foltz, C. B., Chaffee, F. H., & Black, J. H. 1988, ApJ, 324, 267
- Frerking, M. A., Langer, W. D., & Wilson, R. W. 1982, ApJ, 262, 590
- Frerking, M. A., Keene, J., Blake, G., & Phillips, T. G. 1989, ApJ, 344, 311
- Gatley, I., Jones, T. J., Hyland, A. R., Beattie, D. H., and Lee, T. J. 1984, MNRAS, 210, 565.
- Gatley, I., Hasegawa, T., Suzuki, H., Garden, R., Brand, P., Lightfoot, J., Glenncross, W., Okuda, H., and Nagata, T. 1987, ApJ, 318, L73.
- Gautier, T. N., III, Fink, U., Larson, H. P., Treffers, R. R. 1976, ApJ, 207, L129.
- Ge, J. & Bechtold, J. 1997, ApJL, 477, L73
- Ge, J. & Bechtold, J. 1999, ASP Conf. Ser. 156: Highly Redshifted Radio Lines, 121
- Ge, J., Bechtold, J., & Kulkarni, V. P. 2001, ApJL, 547, L1

Gear, W. K. & Cunningham, C. R. 1995, ASP Conf. Ser. 75: Multi-Feed Systems for Radio Telescopes, 215

Geballe, T. R. & Oka, T. 1989, *ApJ*, 342, 855

Geballe, T. R., Jagod, M.-F., & Oka, T. 1993, *ApJL*, 408, L109

Geballe, T. R. & Oka, T. 1996, *Nature*, 384, 334

Geballe, T. R., McCall, B. J., Hinkle, K. H., & Oka, T. 1999, *ApJ*, 510, 251

Gehrz, R. D., Sramek, R. A., Weedman, D. W. 1983, *ApJ*, 267, 551.

Goldsmith, P. F. & Langer, W. D. 1999, *ApJ*, 517, 209

Goldsmith, P. F. et al. 2000, *ApJL*, 539, L123

Goorvitch, D. & Chackerian, C. 1994, *ApJS*, 91, 483

Gould, R. J. & Salpeter, E. E. 1963, *ApJ*, 138, 393

Gould, R. J., Gold, T., & Salpeter, E. E. 1963, *ApJ*, 138, 408

Gould, R. J. & Harwit, M. 1963, *ApJ*, 137, 694

Graham, J. R., Wright, G. S., Longmore, A. J. 1987, *ApJ*, 313, 847.

Graham, J. R., Wright, G. S., & Longmore, A. J. 1990, *ApJ*, 352, 172

Gredel, R., van Dishoeck, E. F., & Black, J. H. 1993, *A&A*, 269, 477

Gredel, R. 1996, *A&A*, 305, 582.

Gredel, R. 1997, *A&A*, 320, 929

Green, S., Ramaswamy, R., & Rabitz, H. 1978, *ApJS*, 36, 483

- Grevesse, N., Lambert, D. L., Sauval, A. J., van Dishoeck, E. F., Farmer, C. B., & Norton, R. H. 1991, *A&A*, 242, 488
- Groppi, C. E., Walker, C. K., Ziurys, L., & Kulesa, C. A. 2003, in preparation
- Habing, H. J. 1968, *Bull. Astron. Inst. Netherlands*, 19, 421
- Haiman, Z. ;, Abel, T., & Rees, M. J. 2000, *ApJ*, 534, 11
- Hartquist, T. W., Dyson, J. E., & Williams, D. A. 1992, *MNRAS*, 257, 419
- Helmich, F. P., Jansen, D. J., de Graauw, T., Groesbeck, T. D., & van Dishoeck, E. F. 1994, *A&A*, 283, 626
- Helmich, F.P., van Dishoeck, E.F., Black, J.H., et al. 1996, *A&A*, 315, 173
- Henry, R. B. C. & MacAlpine, G. M. 1982, *ApJ*, 258, 11
- Herbst, E. & Klemperer, W. 1973, *ApJ*, 185, 505
- Herzberg, G. 1950, New York: Van Nostrand Reinhold, 1950, 2nd ed.,
- Hollenbach, D. J., Werner, M. W., & Salpeter, E. E. 1971, *ApJ*, 163, 165
- Hollenbach, D. & Salpeter, E. E. 1971, *ApJ*, 163, 155
- Hollenbach D., and Shull, J.M. 1977, *ApJ*, 216, 419.
- Hollenbach, D. & McKee, C.F. 1989, *ApJ*, 342, 306.
- Hollenbach, D. J., Takahashi, T., & Tielens, A. G. G. M. 1991, *ApJ*, 377, 192
- Howe, J. E., Jaffe, D. T., Genzel, R., & Stacey, G. J. 1991, *ApJ*, 373, 158
- Hummer, D.G., and P.J. Storey. 1987, *MNRAS*, 224, 801.

- Hutchings, R. M., Santoro, F., Thomas, P. A., & Couchman, H. M. P. 2002, MN-RAS, 330, 927
- Irvine, W. M., Goldsmith, P. F., & Hjalmarson, A. 1987, ASSL Vol. 134: Interstellar Processes, 561
- Jaffe, D. T., Zhou, S., Howe, J. E., Herrmann, F., Madden, S. C., Poglitsch, A., van der Werf, P. P., & Stacey, G. J. 1994, ApJ, 436, 203
- Jenkins, E. B. & Peimbert, A. 1997, ApJ, 477, 265
- Jiang, D. R., Perrier, C., & Lena, P. 1984, A&A, 135, 249
- Johnstone, D., Wilson, C. D., Moriarty-Schieven, G., Joncas, G., Smith, G., Gregersen, E., & Fich, M. 2000, ApJ, 545, 327
- Joseph, R.D., Wright, G.D., and Wade, R. 1984, Nature, 311, 132.
- Jura, M. 1974, ApJ, 191, 375
- Jura, M. 1975, ApJ, 197, 575
- Jura, M. 1975, ApJ, 197, 581
- Jura, M. 1975, ApJ, 202, 561
- Kalberla, P. M. W., Shchekinov, Y. A., & Dettmar, R.-J. 1999, A&A, 350, L9
- Kawara, K., Gregory, B., Nishida, M. 1987, ApJ, 321, L35.
- Kaufman, M. J., Wolfire, M. G., Hollenbach, D. J., & Luhman, M. L. 1999, ApJ, 527, 795
- Keene, J., Blake, G., Phillips, T. G., Huggins, P. J., & Beichman, C. A. 1985, ApJ, 299, 967

- Keene, J. 1987, SETI Conference *Carbon in the Galaxy*
- Kleinmann, S. G. & Hall, D. N. B. 1986, ApJS, 62, 501.
- Knacke, R.F., Geballe, T.R., Noll, K.S., & Tokunaga, A.T. 1985, ApJ, 298, L67
- Köster, B., Störzer, H., Stutzki, J., & Sternberg, A. 1994, A&A, 284, 545
- Kreysa, E. 1992, in: ESA-Symposium on Photon Detectors for Space Instrumentation, Noordwijk, p. 207 (ESA SP-356)
- Kurucz, R. L. 1979, ApJSuppl., 40, 1.
- Kurucz, R. L. 1992, in IAU Symposium 149, The Stellar Populations of Galaxies, ed. B. Barbuy & A. Renzini (Dordrecht:Kluwer), 225.
- Lacy, J.H., Evans, N.J., Achtermann, J.M., Bruce, D.E., Arens, J.F., & Carr, J.S. 1989, ApJ, 342, L43.
- Lacy, J.H., Carr, J.S., Evans, N.J., Baas, F., Achtermann, J.M., & Arens, J.F. 1991, ApJ, 376, 556.
- Lacy, J. H., Knacke, R., Geballe, T. R., & Tokunaga, A. T. 1994, ApJL, 428, L69
- Lada, C. J., Lada, E. A., Clemens, D. P., & Bally, J. 1994, ApJ, 429, 694
- Lambert, D. L., Sheffer, Y., Gilliland, R. L., & Federman, S. R. 1994, ApJ, 420, 756
- Langer, W. D. & Penzias, A. A. 1993, ApJ, 408, 539
- Latter, W. B. & Black, J. H. 1991, ApJ, 372, 161
- Le Bourlot, J., Gerin, M., & Perault, M. 1989, A&A, 219, 279

- le Bourlot, J., Pineau des Forêts, G., Roueff, E., & Flower, D. R. 1993, A&A, 267, 233
- Lee, H.-H., Bettens, R. P. A., & Herbst, E. 1996, A&AS, 119, 111
- Lester, D.F, Harvey, P.M., and Carr, J.S. 1988, ApJ, 352, 544.
- Levshakov, S. A., Chaffee, F. H., Foltz, C. B., & Black, J. H. 1992, A&A, 262, 385
- Liseau, R., White, G., Larsson, B., Sidher, S., Olofsson, G., Kaas, A., Nordh, L., Caux, E., Lorenzetti, D., Molinari, S., Nisini, B., & Sibille, F. 1999, A&A, 344, 342
- Luhman, M. L., Jaffe, D. T., Graham, J. R., Wright, G. S., Hester, J. J., Longmore, A. J. 1991, AJ, 101, 175.
- Luhman, M. L., Jaffe, D. T., Keller, L. D., Pak, S. 1994, ApJ, 436, L185.
- Luhman, M. L., Jaffe, D. T. 1994, ApJ, 463, 191.
- Lumsden, S. L., Puxley, P. J., Doherty, R. M. 1994, MNRAS, 268, 821.
- Lyu, C., Smith, A. M., & Bruhweiler, F. C. 1994, ApJ, 426, 254
- Maillard, J., Drossart, P., Watson, J. K. G., Kim, S. J., & Caldwell, J. 1990, ApJL, 363, L37
- Maiolino, R., Rieke, G. H., and Rieke, M. J. 1996, AJ, 111, 537.
- Malfait, K., Bogaert, E., & Waelkens, C. 1998, A&A, 331, 211
- Maloney, P., and Black, J.H. 1988, ApJ, 325, 389.
- Maloney, P. R., Hollenbach, D. J., & Tielens, A. G. G. M. 1996, ApJ, 466, 561

- Martin, P. G., Mandy, M. E. 1995, ApJ, 455, L89.
- Martin, D. W., McDaniel, E. W., & Meeks, M. L. 1961, ApJ, 134, 1012
- Mauersberger, R., Wilson, T. L., Mezger, P. G., Gaume, R., & Johnston, K. J. 1992, A&A, 256, 640
- McCall, B. J., Geballe, T. R., Hinkle, K. H., & Oka, T. 1999, ApJ, 522, 338
- McCall, B. J. et al. 2002, ApJ, 567, 391
- McLeod, K.K., Rieke, G.H., Rieke, M.J., and D.M. Kelly. 1993, ApJ, 412, 111.
- McGregor, P. J., Persson, S. E., & Cohen, J. G. 1984, ApJ, 286, 609
- Meixner, M., & Tielens, A. G. G. M. 1993, ApJ, 405, 216
- Mihos, J. C., & Hernquist, L. 1996, ApJ, 464, 641.
- Miller, J. S. 1978, ApJ, 220, 490
- Miller, S., Tennyson, J., & Joseph, R. D. 1990, ApJL, 360, L55
- Mitchell, G.F., Curry, C., Maillard, J.-P., & Allen, M. 1989, ApJ, 341, 1020.
- Mitchell, G.F., Maillard, J.-P., Allen, M., Beer, R., & Belcourt, K. 1990, ApJ, 363, 554.
- Mitchell, G. F. & Maillard, J. 1993, ApJL, 404, L79
- Mitchell, G. F., Lee, S. W., Maillard, J., Matthews, H., Hasegawa, T. I., & Harris, A. I. 1995, ApJ, 438, 794
- Monteiro, T. S. 1985, MNRAS, 214, 419
- Moorwood, A. F. M. and Olivia, E. 1994, ApJ429, 602.

- Moos, H. W. et al. 2000, ApJL, 538, L1
- Morton, D. C. 1975, ApJ, 197, 85
- Motte, F., Andre, P., & Neri, R. 1998, A&A, 336, 150
- Mouri, H., Kawara, K., Taniguchi, Y., Nishida, M. 1990, ApJ, 356, 39.
- Nakagawa, T., Nagata, T., Geballe, T. R., Okuda, H., Shibai, H., Matsuhara, H. 1989, ApJ, 340, 729.
- Neale, L., Miller, S., & Tennyson, J. 1996, ApJ, 464, 516
- Nelson, D.D., Schiffman, A. Nesbitt, D.J., Orlando, J.J., Burkholder, J.B. 1990, J. Chem. Phys., 93(10), 7003.
- Nisini, B., Smith, H. A., Fischer, J., & Geballe, T. R. 1994, A&A, 290, 463
- Norman, C. A. & Spaans, M. 1997, ApJ, 480, 145
- Nussbaumer, H. & Storey, P. J. 1988, A&A, 193, 327.
- Oka, T. 1980, Physical Review Letters, 45, 531
- Oka, T. 1981, Phil. Trans. Roy. Soc. London A 303, 543.
- Oka, T. & Geballe, T. R. 1990, ApJL, 351, L53
- Origlia, L., Moorwood, A. F. M. & Oliva, E. 1993, A&A, 280, 536.
- Ossenkopf, V. & Henning, T. 1994, A&A, 291, 943
- Pak, S., Jaffe, D. T., Keller, L. D. 1996, ApJ, 457, L43.
- Peebles, P. J. E. 1993, Princeton Series in Physics, Princeton, NJ: Princeton University Press, —c1993.

- Pineau Des Forêts, G., Roueff, E., & Flower, D. R. 1992, MNRAS, 258, 45P
- Plume, R., Jaffe, D. T., Tatematsu, K., Evans, N. J., & Keene, J. 1999, ApJ, 512, 768
- Prasad, S. S., Tarafdar, S. P., Villere, K. R., & Huntress, W. T. 1987, ASSL Vol. 134: Interstellar Processes, 631
- Preibisch, T., Ossenkopf, V., Yorke, H. W., & Henning, T. 1993, A&A, 279, 577
- Norman, C., in: Pudritz, R. E. & Fich, M. (eds.) 1988, NATO ASIC Proc. 232: Galactic and Extragalactic Star Formation
- Puxley, P. J. Hawarden, T. G., and Mountain, M. C. 1988, MNRAS, 234, 29.
- Puxley, P. J. Hawarden, T. G., and Mountain, M. C. 1990, ApJ, 364, 77.
- Rachford, B. L. et al. 2001, ApJ, 555, 839
- Rachford, B. L. et al. 2002, ApJ, 577, 221
- Richter, M. J., Graham, J. R., Wright, G. S., Kelly, D. M., Lacy, J. H. 1995, ApJ, 449, 83.
- Rieke, G. H. & Lebofsky, M. J. 1985, ApJ, 288, 618
- Rieke, G.H., Cutri, R.M., Black, J. H., Kailey, W. F., McAlary, C. W., Lebofsky, M. J., and Elston, R. 1985, ApJ, 290, 116.
- Roche, P. F. & Aitken, D. K. 1984, MNRAS, 208, 481
- Rogerson, J. B., Spitzer, L., Drake, J. F., Dressler, K., Jenkins, E. B., Morton, D. C., & York, D. G. 1973, ApJL, 181, L97

- Salpeter, E. E. 1955, ApJ, 121, 161.
- Sargent, A., Scoville, N. 1991, ApJ, 366, L1.
- Sargent, A. I., Sanders, D. B., Scoville, N. Z., Soifer, B. T. 1987, ApJ, 312, L35.
- Scalo, J.M. 1986, Fund. Cosmic Phys., 11, 1.
- Schaerer, D., de Koter, A., Schmutz, W., Maeder, A. 1996, A&A, 310, 837.
- Schaerer, D., de Koter, A., Schmutz, W., Maeder, A. 1996, A&A, 312, 475.
- Schaerer, D. & de Koter, A. 1997, A&A, 322, 598.
- Schaller, G., Schaerer, D., Meynet, G., Maeder, A. 1992, A&ASuppl., 96, 269.
- Schaefer, J. 1999, H<sub>2</sub> in Space, meeting held in Paris, France, September 28th - October 1st, 1999. Eds.: F. Combes, G. Pineau des Forets. Cambridge University Press, Astrophysics Series,
- Schieder, R., Tolls, V., & Winnewisser, G. 1989, Experimental Astronomy, 1, 101
- Schinke, R., Engel, V., Buck, U., Meyer, H., & Diercksen, G. H. F. 1985, ApJ, 299, 939
- Scoville, N. Z., Hall, D. N. B., Ridgway, S. T., & Kleinmann, S. G. 1979, ApJL, 232, L121
- Seaton, M.J. 1978, MNRAS, 187, 73P
- Shields, J. C. 1993, ApJ, 419, 181.
- Shier, L. M., Rieke, M. J., Rieke, G. H. 1994, ApJ, 433, L9.
- Shier, L. M. 1995, PhD Thesis, University of Arizona, Tucson, AZ.

- Shchekinov, Y., Dettmar, R.-J., & Shchekinov, Y. A. 1999, H<sub>2</sub> in Space, meeting held in Paris, France, September 28th - October 1st, 1999. Eds.: F. Combes, G. Pineau des Forêts. Cambridge University Press, Astrophysics Series,
- Shu, F. H. 1977, ApJ, 214, 488
- Shu, F. H., Adams, F. C., & Lizano, S. 1987, ARA&A, 25, 23
- Shuping, R. Y., Snow, T. P., Chiar, J. E., & Kerr, T. 2000, ApJ, 529, 932
- Shuping, R. Y., Chiar, J. E., Snow, T. P., & Kerr, T. 2001, ApJL, 547, L161
- Smith, M. D. 1994, A&A, 289, 256.
- Solomon, P. M., Downes, D., Radford, S. J. E. 1992, ApJ, 387, L55.
- Solomon, P. M. & Wickramasinghe, N. C. 1969, ApJ, 158, 449
- Somerville, W. B. 1970, MNRAS, 147, 201
- Spaans, M. 1996, A&A, 307, 271
- Stark, A. A. et al. 2001, PASP, 113, 567
- Stacey, G. J., Geis, N., Genzel, R., Lugten, J. B., Poglitsch, A., Sternberg, A., Townes, C. H. 1991, ApJ, 373, 423.
- Sternberg, A., and Dalgarno, A. 1989, ApJ, 338, 197.
- Stecher, T. P. & Williams, D. A. 1966, ApJ, 146, 88
- Stecher, T. P. & Williams, D. A. 1967, ApJL, 149, L29
- Stutzki, J., Stacey, G. J., Genzel, R., Harris, A. I., Jaffe, D. T., & Lugten, J. B. 1988, ApJ, 332, 379

- Sundström, G., et al. 1994, *Science*, 263, 785
- Tauber, J. A. & Goldsmith, P. F. 1990, *ApJL*, 356, L63.
- Telesco, C. M., Decher, R. & Gatley, I. 1985, *ApJ*, 299, 896.
- Tielens, A. G. G. M. & Hollenbach, D. 1985, *ApJ*, 291, 722
- Tielens, A. G. G. M., and Hollenbach, D. 1985, *ApJ*, 291, 747.
- Treffers, R. R., Fink, U., Larson, H. P., Gautier, T. N., III. 1976, *ApJ*, 209, 793.
- Treffers, R. R. 1979, *ApJ*, 233, 17.
- Scott, G. B. I., Fairley, D. A., Freeman, C. G., & McEwan, M. J. 1997, *Chem. Phys. Lett.*, 269, 88
- Spaans, M. PhD Thesis, Leiden University, 1995.
- Spitzer, L., Cochran, W. D., & Hirshfeld, A. 1974, *ApJS*, 28, 373
- Spitzer, L. & Jenkins, E. B. 1975, *ARA&A*, 13, 133
- Spitzer, L. 1978, New York Wiley-Interscience, 1978. 333 p.
- Schwartz, R. D. 1983, *ApJ*, 268, L37.
- Schwartz, R. D., Cohen, M., Williams, P. M. 1987, *ApJ*, 322, 403.
- Schwartz, R. D., Jennings, D. G., Williams, P. M., Cohen, M. 1988, *ApJ*, 334, 99.
- Snow, T. P. et al. 2000, *ApJL*, 538, L65
- Shull, J. M. & Beckwith, S. 1982, *ARA&A*, 20, 163
- Stahl, O., Appenzeller, I., Wilson, T. L., & Henkel, C. 1989, *A&A*, 221, 321

- Strömgren, B. 1939, ApJ, 89, 526
- Thompson, R. I., Lebofsky, M. J., and Rieke, G. H. 1978, ApJ, 222, L49.
- Thompson, R. I., Thronson, H. A., & Campbell, B. G. 1981, ApJ, 249, 622
- Thronson, H. A., Schwartz, P. R., Smith, H. A., Glaccum, W., Harper, D. A., Loewenstein, R. F., Smith, J., & Lada, C. J. 1984, ApJ, 280, 154
- Tielens, A. G. G. M. & Hollenbach, D. 1985, ApJ, 291, 722
- Tine, S., Lepp, S., Gredel, R., & Dalgarno, A. 1997, ApJ, 481, 282
- Trafton, L. M., Geballe, T. R., Miller, S., Tennyson, J., & Ballester, G. E. 1993, ApJ, 405, 761
- Valentijn, E. A., van der Werf, P. P., de Graauw, Th., de Jong, T. 1996, A&A, 315, 145.
- van Dehulst, H. C. 1949, Utrecht, Drukkerij Schotanus & Jens, 1949., 2
- van der Tak, F. F. S. & van Dishoeck, E. F. 2000, A&A, 358, L79
- van Dishoeck, E. F. & de Zeeuw, T. 1984, MNRAS, 206, 383
- van Dishoeck, E. F. & Black, J. H. 1986, ApJS, 62, 109
- van Dishoeck, E. F., and Black, J. H. 1988, ApJ, 334, 771.
- van Dishoeck, E.F., Black, J.H., Phillips, T.G., & Gredel, R. 1991, ApJ, 366, 141.
- van Dishoeck, E.F. & Helmich, F.P. 1996, A&A, 315, 177.
- van Dishoeck, E.F., Helmich, F.P., de Graauw, Th., Black, J.H., et al. 1996, A&A, 315, 349.

- Vanzi, L. & Rieke, G. H. 1997, *ApJ*, 479, 694.
- Wall, W.F., Jaffe, D. T., Bash, F. N., Israel, F. P. 1991, *ApJ*, 380, 384.
- Wall, W. F., Jaffe, D. T., Bash, F. N., Israel, F. P., Maloney, P. R., Baas, F. 1993, *ApJ*, 414, 98.
- Walker, C. K., Kooi, J., & Jacobs, K. 2002, in preparation.
- Wannier, P. G., Penzias, A. A., & Jenkins, E. B. 1982, *ApJ*, 254, 100
- Watson, W. D. 1976, *ApJ*, 204, 47
- Watson, D. M., Genzel, R., Townes, C. H., & Storey, J. W. V. 1985, *ApJ*, 298, 316
- Werner, M. W. & Harwit, M. 1968, *ApJ*, 154, 881
- Werner, M. W. 1969, *ApJ*, 156, 753
- Williams, D. M., Thompson, C. L., Rieke, G. H., Montgomery, E. F. 1993, SPIE, 1946, 482.
- Wilking, B. A., Schwartz, R. D., Mundy, L. G., Schultz, A. S. B. 1990, *AJ*, 99, 344.
- Wilking, B. A. & Lada C. J. 1983, *ApJ*, 274, 698
- Wilson, T. L., Serabyn, E., Henkel, C., & Walmsley, C. M. 1986, *A&A*, 158, L1
- Wilson, T. L., Mauersberger, R., Langer, W. D., Glassgold, A. E., & Wilson, R. W. 1992, *A&A*, 262, 248
- Wilson, T. L. & Rood, R. 1994, *ARA&A*, 32, 191
- Wilson, C. D. et al. 1999, *ApJL*, 513, L139
- Wilson, R. W., Jefferts, K. B., & Penzias, A. A. 1970, *ApJL*, 161, L43

- Witt, A. N., Thronson, H. A., Jr., Capuano, J. M., Jr. 1992, ApJ, 393, 611.
- Wolniewicz, L., Simbotin, I., & Dalgarno, A. 1998, ApJS, 115, 293
- Wootten, H. A., <http://www.cv.nrao.edu/~awootten/allmols.html>
- Wynn-Williams, C. G., Eales, S. A., Hodapp, K. W., Joseph, R. D., McLean, I. S., Simmons, D. S., & Wright, G. S. 1991, ApJ, 377, 426.
- Wu, C.-C. 1981, ApJ, 245, 581
- Young, J. S., Claussen, M. J., Kleinmann, S. G., Rubin, V. C., Scoville, N. 1988, ApJ, 331, 81.
- Ziurys, L. M. & Turner, B. E. 1986, ApJL, 300, L19
- Zmuidzinas, J. & LeDuc, H. G. 1999, IEEE Trans. Microwave Theory Tech., 40, 1797